Effects of Olefin Group and Its Position on the Kinetics for Intramolecular H-Shift and HO2 Elimination of Alkenyl Peroxy Radicals

ARTICLE *in* THE JOURNAL OF PHYSICAL CHEMISTRY A · FEBRUARY 2011

Impact Factor: 2.69 · DOI: 10.1021/jp1111839 · Source: PubMed

2 AUTHORS:

Feng Zhang
University of Science and Technology of China
36 PUBLICATIONS **291** CITATIONS
SEE PROFILE

Theodore S Dibble
State University of New York College of Envir…
79 PUBLICATIONS **1,026** CITATIONS
SEE PROFILE

THE JOURNAL OF PHYSICAL CHEMISTRY A

ARTICLE

pubs.acs.org/JPCA

Effects of Olefin Group and Its Position on the Kinetics for Intramolecular H-Shift and HO_2 Elimination of Alkenyl Peroxy Radicals

Feng Zhang and Theodore S. Dibble*

Department of Chemistry, College of Environmental Science and Forestry, State University of New York, Syracuse, New York 13210, United States

Supporting Information

ABSTRACT: Two classes of unimolecular reactions of peroxy radicals are key to autoignition, namely, intramolecular H-atom shift (which promotes autoignition) and concerted HO_2 elimination (which inhibits autoignition). Olefin groups are prominent functional groups in biodiesel fuels. This paper explores the effects of the presence of an olefin group and its position on the kinetics of unimolecular reactions of peroxy radicals. CBS-QB3 calculations were carried out for 10 selected alkyl- and alkenylperoxy radicals. Transition-state theory was used to determine the temperature dependence of the high-pressure limiting rate constants, and Rice−Ramsperger−Kassel−Marcus/master equation simulations were performed to determine the pressure dependence of selected rate constants. Tunneling effects were computed using the asymmetric Eckart potential. The contribution of internal rotors to partition functions were included by using the hindered-rotor treatment.

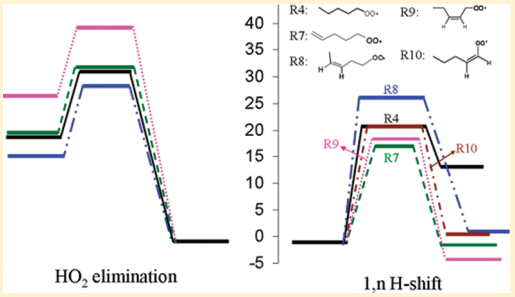

1. INTRODUCTION

Biodiesel fuel is increasingly being used worldwide for its expected environmental benefits. It is typically composed of mixtures of fatty acid methyl esters (FAMEs), which contain olefin and ester groups.[1] Ester groups and nonaromatic double bonds are largely absent from traditional petroleum diesel fuel, which is mostly composed of large alkanes and *n*-alkyl-substituted aromatic hydrocarbons.[2] Diesel ignition occurs via the spontaneous combustion (autoignition) of fuel injected into air that has been heated by compression.[3] Peroxy radicals are critical intermediates in autoignition of diesel fuel,[4−6] but the effect of the functional groups in FAMEs on biodiesel ignition has scarcely been studied.

The ignition of diesel fuel depends on isomerization of peroxy radicals via intramolecular hydrogen atom abstraction (1,*n* H-shift); e.g.,

$$CH_3CH_3CH_2OO^{\bullet} \rightarrow {}^{\bullet}CHCH_3CH_2OOH \qquad (R1)$$

The products of these reactions are generically referred to as QOOH. Production of multiple OH radicals (chain branching) in the chemistry following reaction R1 leads to autoignition.[7] However, other reactions compete with the 1,*n* H-shift and consequently delay the autoignition,[8] such as

$$ROO^{\bullet} \rightarrow \text{products} + HOO^{\bullet} \qquad (R2)$$

Understanding of the kinetics and thermodynamics of these unimolecular reactions is crucial for combustion chemistry. $CH_3CH_2OO^{\bullet}$ is the prototype for the competition between reactions R1 and R2 and has been exhaustively studied in both experiments and calculations.[9−21] A number of studies have treated larger alkylperoxy radicals.[22−33] A recent review by Taatjes illustrates how real-time spectroscopic monitoring, combined with quantum chemistry and statistical rate theory, has confirmed and extended the conclusions of older experimental work that was largely based on product yield analyses.[27]

Although there is substantial literature on the fundamental chemistry of peroxy radicals derived from saturated hydrocarbon species, researchers have only very recently carried out similar investigations for peroxy radicals from biodiesel fuel (or models thereof). Lee and Bozzelli analyzed the thermochemical properties and kinetics for the allyl radical ($CH_2{=}CHCH_2^{\bullet}$) + O_2 reaction system by quantum chemistry and Rice−Ramsperger−Kassel−Marcus (RRKM)/master equation simulations.[34] Recently, Miyoshi theoretically investigated the oxidation of 3-butenyl ($^{\bullet}CH_2CH_2CH{=}CH_2$) radical and subsequent unimolecular reactions of 3-butenylperoxy radical.[35] The need for more study is confirmed by the extensive assumptions needed in kinetic modeling studies of combustion of alkenes. For example, Bounaceur et al. investigated the influence of the position of the double bond on the autoignition of linear hexenyl and pentenyl radicals.[36] They modeled the most stable *trans*-alkenes, assuming cis conformers were less important. However, most natural fatty acids are in cis configurations.[37] Similarly, Mehl and co-workers[38]

Received: August 6, 2010
Revised: December 16, 2010
Published: January 14, 2011

Scheme 1. Intramolecular H-Shift and HO_2 Elimination Reactions Treated in This Work

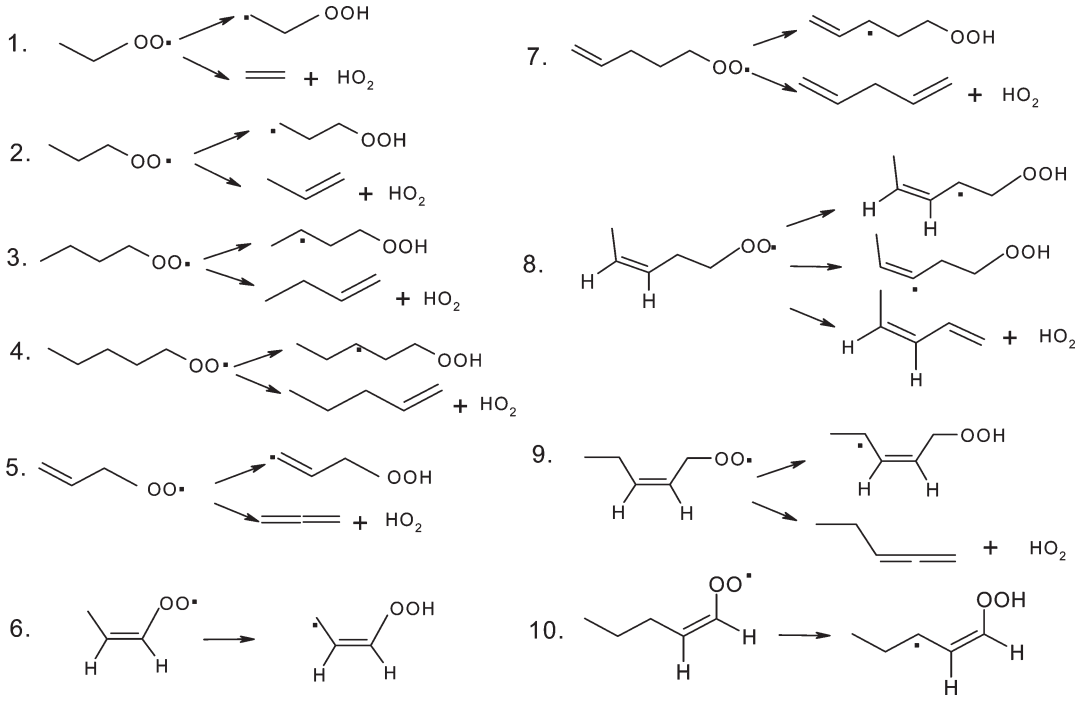

were forced to make several assumptions about the quantitative effect of double bonds on peroxy radical kinetics in order to construct their model for *n*-hexene autoignition, and the present work allows the validity of these assumptions to be checked. Clearly, much more extensive and systematic theoretical studies of peroxy radicals with olefin functionality are needed to understand the autoignition of biodiesel fuel. In this work, quantum chemical calculations and RRKM/master equation methods are used to explore the effects of olefin groups and their positions on the barrier heights and kinetics of the intramolecular H-shift and concerted HO_2 elimination reactions of peroxy radicals (note that this paper only considers direct HO_2 production, not production from $ROO^{\bullet} \rightarrow \beta$-QOOH $\rightarrow HO_2$ + alkene). For alkylperoxy radicals, 1,5 H-shift reactions take place through a six-member cyclic transition state, typically providing a lower activation barrier than smaller (strained) transition states[20,28,29,39] and a lower activation entropy than H-shifts occurring through larger transition states.[28,29,40] As the first step in our series of studies on model molecules for biodiesel, and because they are the most important reactions, the present study focuses on the 1,*n* H-shift channels with the lowest barrier (1,5 H-shift for most systems). Scheme 1 shows the specific unimolecular reactions addressed in this work. cis conformers are used for alkenylperoxy radicals.

2. COMPUTATIONAL DETAILS

For all 10 reactants shown in Scheme 1, geometries of all possible conformers were optimized by molecular mechanics using the Spartan program[41] (for alkenes, only the specified configuration was considered). The resulting geometries were optimized by the recently developed M05-2X functional,[42] which has been optimized for kinetics and thermodynamics.[43,44] The 6-31+G(d,p) basis set was employed, and calculations for free radicals were carried out with the spin-unrestricted formalism. The six conformers with the lowest M05-2X/6-31+G(d,p) energies (including zero-point energy correction) were reoptimized by the CBS-QB3[45] method to determine the minimum energy conformation. The optimization of transition states and products also starts from the M05-2X/6-31+G(d,p) geometry, followed by composite CBS-QB3 calculation. The CBS-QB3 method starts by optimizing geometries and determining harmonic vibrational frequencies at B3LYP/6-311G(d,p). This is followed by CCSD(T)/6-31+G(d') single points, extrapolation of the MP2 correlation energy to the basis set limit, and addition of an empirical correction term.[45] CBS-QB3 has been widely used to explore peroxy radical chemistry.[28,29,46−49] In CBS-QB3 calculations, the B3LYP/6-311G(d,p) zero-point energy (ZPE) is scaled by a factor 0.99; for the RRKM calculations the vibrational frequencies were scaled by a factor of 0.97.[49] The nature of saddle points was checked by vibrational analysis. All ab initio calculations were performed by a Gaussian 09 program package.[50] It should be noted that the 1,5 H-shift reactions of R6 and R10 can only occur from the cis isomers, while the HO_2 elimination is not feasible for the cis isomers of these species. It is well-known that the cis→trans isomerization for alkenes has very high barrier, e.g., ∼66 kcal/mol for butene and pentene.[51] Therefore, as shown in Scheme 1, only the cis isomers are considered. For the same reason, the cis isomer is used for R9, instead of the trans isomer.

High-pressure limiting (HPL) rate constants and their dependence on temperature were calculated by transition-state theory, using the program package UNIMOL,[52] as modified by Miyoshi.[53] The pressure dependence of rate constants was given by an energy-grained RRKM/master equation analysis within UNIMOL;[52,53] energy grains of 10 cm^{-1} rather than the default 100 cm^{-1} were used to minimize numerical error. Collisional

dx.doi.org/10.1021/jp1111839 |*J. Phys. Chem. A* 2011, 115, 655–663

Table 1. Activation Barriers (E_0, 0 K, kcal/mol) and Reaction Energies (ΔE_{reacn}, 0 K, kcal/mol) and Imaginary Vibrational Frequencies (ν^*, cm^{-1}) at the CBS-QB3 Level of Theory

	1,*n* H-shift[a]			HO_2 elimination		
reactants	E_0	ΔE_{reacn}	ν_*	E_0	ΔE_{raecn}	ν_*
R1	36.0	16.9	2274	31.2	20.6	1098
	37.3[b]	**16.5**[b]	**2273**[c]	**30.4**[b]	**17.2**[b]	
	36.9[d]	**16.8**[d]		**30.8**[d]	**21.1**[d]	
	33.0[e]	**15.4**[e]		**30.9**[e]	**19.2**[f]	
	35.9[c]			**30.0**[f]		
R2	23.8	15.9	1637	30.9	18.2	1033
	23.4[c]	**14.1**[g]	**1637**[c]	**30.1**[g]		
	22.7[g]	**15.9**[h]		**30.9**[h]		
	23.9[h]					
R3	21.1	13.2	1696	30.7	18.7	1045
	20.6[c]	**13.8**[i]		**30.0**[i]	**18.9**[i]	
	22.3[i]	**12.9**[j]		**30.8**[j]		
	21.0[j]					
R4	20.7	13.5	1680	30.6	18.8	1046
R5	29.1	25.6	1318	40.2	26.2	1080
	28.9[k]	**25.8**[k]		**36.6**[k]	**26.5**[k]	
R6	24.0	*-0.2*[l,n]	1763		–	
R7	17.3	−0.9	1775	31.4	19.6	1059
R8	26.0 (26.0)[m]	1.4 (21.8)[m]	2156 (1461)[m]	28.1	15.6	1022
R9	19.8	−2.2	1761	38.8	26.2	1062
R10	20.8	*-0.2*[l,n]	1731		–	

[a] n = 4 for R1 and R8, n = 6 for R9, and n = 5 for other species. [b] Reference 14 at the CCSD(T)/TZ2P//CCSD(T)/DZP level. [c] Reference 32 (Sharma) at CBS-QB3 level. [d] Reference 18 at "G2-like" level. [e] Reference 20 at CBS-QB3//B3LYP/6-31G(d,p) level. [f] Reference 17 by focal point analysis. [g] Reference 23 and ref 26 at the level of combination of QCISD/6-31G(d) and MP2/6-311++G(3df,3pd), adjusted to fit experimental data. [h] Reference 28 at the CBS-QB3 level. [i] Reference 23 at the level of combination of QCISD/6-31G(d) and MP2/6-311++G(2df,2pd). [j] Reference 35 (Miyoshi) at the CBS-QB3 level. [k] Reference 34 at the CBS-Q//B3LYP/6-31G(d,p) level. [l] ZPE (M05-2X/6-31G(d,p))+ single-point energy at CBS-QB3 for product (see text for explanation). [m] Values for 1,5 H-shift in parentheses. [n] Reaction energies computed in the present work by CBS-QB3 using M052X geometries and frequencies are shown in italic font.

energy transfer was treated with an exponential-down model. The average energy transferred in deactivating collisions, $\langle \Delta E_{down} \rangle$, was taken to be proportional to the temperature using the proportionality constant of 0.4 cm^{-1}/K, which means $\langle \Delta E_{down} \rangle$ was 400 cm^{-1} at 1000 K. The GPOP program[54] was used to extract information from Gaussian output files and create formatted UNIMOL input files. The buffer gas was assumed to be N_2, and interaction between radicals and buffer gas was modeled by the Lennard-Jones potential. The Lennard-Jones parameters for collisions between reactants (R) and N_2 (M) were obtained by the following rules, as suggested by Gilbert and Smith.[55]

$$\sigma_{RM} = \frac{1}{2}(\sigma_R + \sigma_M) \quad (1a)$$

$$\varepsilon_{RM} = \sqrt{\varepsilon_R \varepsilon_M} \quad (1b)$$

The Lennard-Jones parameters for N_2 are available in the early literature.[55,56] For peroxy radicals, these values are estimated by

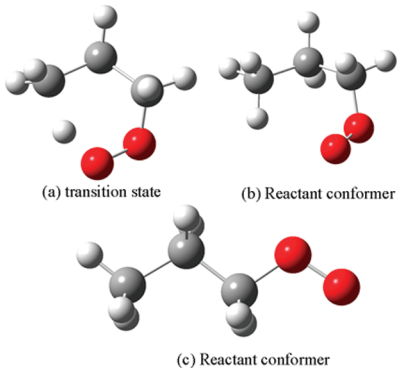

Figure 1. Geometries for 1,5 H-shift of *n*-propylperoxy radical: (a) transition state; (b) minimum reactant conformer at CB3-QB3; (c) reactant conformer used in ref 32.

following empirical formulas:[55,56]

$$\sigma_R = 1.45\left(\sum V_i\right)^{1/3} \quad (2a)$$

$$\varepsilon_R(K) = 1.21 T_b \quad (2b)$$

Here V_i is the additive volume increment of each atom as tabulated in refs 55 and 56 and T_b is the normal boiling point of each species. Since T_b values for peroxy radicals are not known, we used the normal boiling points of the *n*-alkanoic acids with the same number of carbon atoms.[57] This choice is somewhat arbitrary; however, we found that the influence of the T_b value on the calculated rate constant is entirely negligible. The resulting σ_R and ε_R values are listed in the Supporting Information. One-dimensional Eckart tunneling corrections[58,59] were included in calculating both HPL and pressure-dependent rate constants. Internal rotors have important effects to the rate constants of peroxy radical reactions.[32,35] Most reactants and transition states in Scheme 1 have internal rotors, which should be treated as hindered rotors. Some internal motions involve more than one torsion or a mixture of torsion and bending; only those internal rotors which are fairly localized are treated as hindered rotors in this work. Rotational barrier heights were calculated at CBS-QB3. The vibrational modes replaced by hindered rotors and their rotational barrier heights are given in the Supporting Information. The partition functions for hindered rotors were estimated by the Pitzer−Gwinn approximation.[60]

To ease the representation of the relationships between HPL thermal rate constants and temperature, modified Arrhenius rate expressions for HPL rate constants, k_∞, were determined by a nonlinear least-squares fit:

$$k_\infty(T) = A_\infty T^n e^{-E_a/RT} \quad (3)$$

3. RESULTS AND DISCUSSIONS

3.1. Comparison with Previous Literature. A. Quantum Chemical Calculations. Activation and reaction energies and imaginary frequencies at CBS-QB3 are listed in Table 1 for all the investigated unimolecular reactions. Previously computed results for these reactions are included for comparison. Our work reproduces the previous two CBS-QB3 results[28,35] for *n*-propylperoxy (R2) and *n*-butylperoxy results (R3) very well. Figure 1 shows the CBS-QB3 optimized geometries of R2 in our work and

Table 2. HPL Rate Constants (s^{-1}) of 1,*n* H-Shift[a] and HO_2 Elimination Reactions for Peroxy Radicals in the Temperature Range of 300−2500 K (Fitted by the Modified Arrhenius Equation)

	1,*n* H-shift [a]			HO_2 elimination		
reactants	*A*	*x*	E_a/R	*A*	*x*	E_a/R
R1	1.001×10^{-2}	4.007	12 964	1.070×10^{7}	1.679	14 745
R2	1.797×10^{6}	1.729	10 167	2.074×10^{10}	0.901	15 442
R3	4.615×10^{6}	1.558	8 821	4.525×10^{11}	0.585	15 305
R4	7.599×10^{6}	1.472	8 756	1.844×10^{9}	1.103	14 896
R5	5.111×10^{5}	1.698	13 414	2.452×10^{6}	1.822	19 344
R6	3.966×10^{3}	2.392	9 400		−	
R7	1.121×10^{5}	2.005	6 105	1.032×10^{10}	1.053	15 416
R8−14s	9.820×10	2.655	9 172	3.168×10^{10}	0.637	13 887
R8−15s	1.018×10^{8}	1.028	12 196			
R9	4.467×10^{4}	1.292	7 170	9.697×10^{12}	0.200	19 620
R10	6.792×10^{4}	2.058	8 311		−	

[a] *n* = 4 for R1, *n* = 6 for R9, and *n* = 5 for other reactants except R8.

Sharma's,[32] along with the transition state of the 1,5 H-shift of R2. As can be seen in Figure 1, Sharma used a reactant conformer with C_s symmetry. It can be inferred from Table 1, and we verify by direct calculation, that the conformer used by Sharma is 0.5 kcal/mol above the lowest energy conformer. Small discrepancies in calculated reaction energies between the present CBS-QB3 calculations and those of Miyoshi's[35] on R3 may be caused by using different conformers of reaction products. Taatjes and co-workers recently conducted new experiments to validate and improve their previously calculated relative energies[24] for propylperoxy oxidation.[26] They report the barrier height for 1,5 H-shift and HO_2 elimination for *n*-propylperoxy radical as 22.7 kcal/mole and 30.1 kcal/mol, which are close to our CBS-QB3 values of 23.8 and 30.9 kcal/mol, respectively.

There is appreciable scatter (17.2−21.1 kcal/mol) in computed values of the reaction energy for HO_2 elimination from ethylperoxy radical (R1).[14,17,18] Recently Wilke et al.[17] performed a focal point analysis on this reaction, the results of which can be treated as a benchmark for quantum chemical studies of this system. Our values of 31.2 and 20.6 kcal/mol for the barrier height and reaction energy are somewhat higher than their values of 30.0 and 19.2 kcal/mol, respectively.

In calculations for R1 and R5, Bozzelli and co-workers[20,34] modified the CBS-QB3 approach to use 6-31G(d,p) rather than 6-311G(d,p) in B3LYP optimization. This seemingly small change in method lowered the barrier heights of the HO_2 elimination of R5 and 1,5 H-shift of R1 by ∼3 kcal/mol in comparison with standard CBS-QB3 results, although the other two barrier heights determined this way were largely unaffected. The sensitivity of CBS-QB3 activation barriers to the choice of saddle point geometry is illustrated in Figure 2 of ref 32.

As a side note, we examined the correlation between relative energies calculated by M05-2X/6-31+G(d,p) and by CBS-QB3. Combining activation barriers and reaction enthalpies at 0 K, the relative energies (kcal/mol) at the two different levels of theory satisfy the following linear equation with $r^2 = 0.9966$.

$$E_{\text{CBS-QB3}} = 0.928E_{\text{MO5-2X}} - 0.7728 \quad (4)$$

The biggest deviation is 1.4 kcal/mol. Clearly, the M05-2X/6-31+G(d,p) relative energies show a very good correlation with those from CBS-QB3, albeit a systematic overestimation of the barrier heights and reaction energies.

It should be noted that for the reactants R6 and R10, converged geometries of the QOOH products of 1,5 H-shift could not be optimized at B3LYP to start the CBS-QB3 calculation. Instead of the expected QOOH geometries, optimization broke the O−O bond to form an OH radical donating a hydrogen bond to the carbonyl oxygen, that is, CH_2═CHCH=O···HO• and C_2H_5CH═CHCH=O···HO• for R6 and R10, respectively. Geometries of the QOOH species were successfully optimized at the M05-2X/6-311G(d,p) level, but the barrier for breaking the O−O bond is only 0.8−1.0 kcal/mol (including the ZPE correction). The instability of similar hydroperoxy alkyl radicals has been described in previous work.[20,32,61] These minima on the M05-2X/6-311G(d,p) potential energy surface may be artifacts of the method. Even if these two QOOH species are potential energy minima, their production with ∼20 kcal/mol of internal energy will cause them to be very short-lived. However, even QOOH structures that are not minima can occupy a sufficient volume of phase space to live for hundreds of femtoseconds,[62] which is long enough that tunneling can occur to their region of phase space. Since calculation of the tunneling correction by the Eckart method requires the energy of reaction, it is necessary for us to evaluate the energy of these QOOH species. For this reason, we still write the products for 1,5 H-shift of R6 and R10 as the corresponding QOOH species. To obtain energies of these QOOH species at a level consistent with CBS-QB3, CBS-QB3 single-point energy calculations were calculated at the M05-2X/6-311G(d,p) geometry. The M05-2X/6-311G(d,p) ZPE was scaled by 0.965 [63] to compute the energy we report as CBS-QB3. This variation from the standard CBS-QB3 method also is noted in Table 1. The frequencies at M05-2X/6-311G(d,p) are scaled by 0.94 for RRKM/master equation calculations.[63]

B. Kinetics. Although the potential energy profiles provide qualitative insights into kinetics, thermal rate constants must be computed for a more complete understanding. HPL rate constants are represented in the form of a modified Arrhenius equation (eq 3) and have been listed in Table 2. Temperature-dependent rate constants for HO_2 elimination from $C_2H_5OO^•$ and $C_3H_7OO^•$ at several pressures were obtained by Taatjes and co-workers on the basis of a combination of experimental and computational efforts.[24,26] These phenomenological rate constants[64,65] apply to chemically activated ROO• formed in R• + O_2 reactions. Our master equation simulations assume a steady supply of Boltzmann populated ROO•, so it is not appropriate to compare our computed rate constants directly with Taatjes'. The activation barriers determined from Taatjes' work were compared with our results above.

Instead, we make an effort to validate our calculations by comparing with previous theoretical studies on kinetics of alkylperoxy radicals.[29,32,34,35,40] Figure 2 illustrates the comparison between this work and the other three theoretical studies[29,32,35] on the 1,5 H-shift of R3 (1-butylperoxy radical). All four sets of rate constants are based on CBS-QB3 energies. The use of a reactant conformer whose energy is 0.5 kcal/mol higher than the minimum,[32] discussed above, will have a modest effect on the rate constants shown in Figure 2. These four works treated torsions by different methods: Sharma took into account coupled torsional modes by a sophisticated and very time-consuming treatment.[32] Zhu et al. treated all three torsional

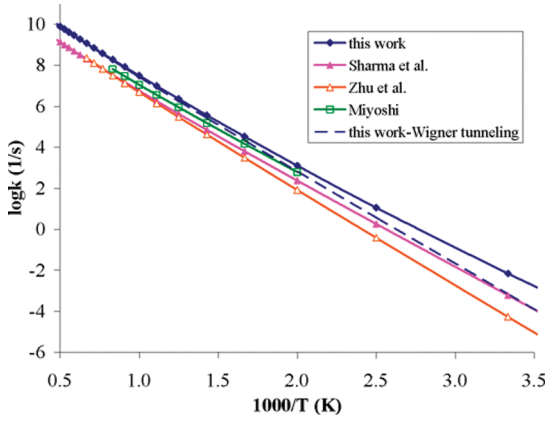

Figure 2. Comparison between this work and previous theoretical studies of Sharma,[32] Zhu, et al.[29] and Miyoshi[35] on rate constants for 1,5 H-shift of *n*-butylperoxy radical (R3).

modes as uncoupled internal rotors.[29] Miyoshi included the contribution of all conformers to the reactant partition function, treating all torsions as harmonic oscillators.[35] In this work, we only consider the effect of internal rotation for those torsional modes recognized as hindered rotors by a subroutine in the GPOP program suite;[54] these are characterized in the Supporting Information. Because a different reactant conformer was used in Sharma's work, the identification of torsional modes could also be different from the others, and that will also affect the calculated rate constants.

In the present work and ref 35, tunneling effects were computed by the asymmetric Eckart potential, but the Wigner formula[66] was used in refs 29 and 32. The blue dashed line in Figure 2 shows the rate constants for 1,5 H-shift of R3 computed in this work but corrected by Wigner tunneling, with the imaginary frequency scaled by 0.70 as suggested by Zhu et al.[29] The disagreement of the Eckart and Wigner tunneling corrections is significant at low temperature (<700 K). The Wigner tunneling correction is more simplistic than the Eckart, but computationally demanding calculations of multidimensional tunneling are required to obtain the reliable tunneling effects.[67,68] For purposes of this paper, the illustration in Figure 2 of the effect of Wigner versus Eckart tunneling on our computed rate constants allows a more direct identification of other sources of differences between our computed rate constants and those of the three other papers.

In the temperature range 300−2000 K, the calculated rate constants in these four studies differ by as much as an order of magnitude, with the largest difference at low temperature. The limitations of the treatment of internal rotors in this work leads to rate constants a factor of 5 higher than Sharma's and Zhu's.[29,32] While accurate activation energies, tunneling corrections, and internal rotor treatment all strongly affect computed rate constants, we regard the limitations of the methodology described in section 2 as acceptable because this paper focuses on the relationship between structure and reactivity of alkenylperoxy radicals rather than obtaining the most accurate rate constants.

We note here that our computed rate constants for the 1,5 H-shift reactions of R2−R4 are in reasonable agreement with (~3.7−6.3 times higher than) those derived from reaction rate rules for 700 K < T < 1000 K.[38]

3.2. Effects of Olefin Group and Its Position. A. Potential Energy Surfaces. To explore the effect of an olefin group and its position on the intramolecular H-transfer and HO_2 elimination

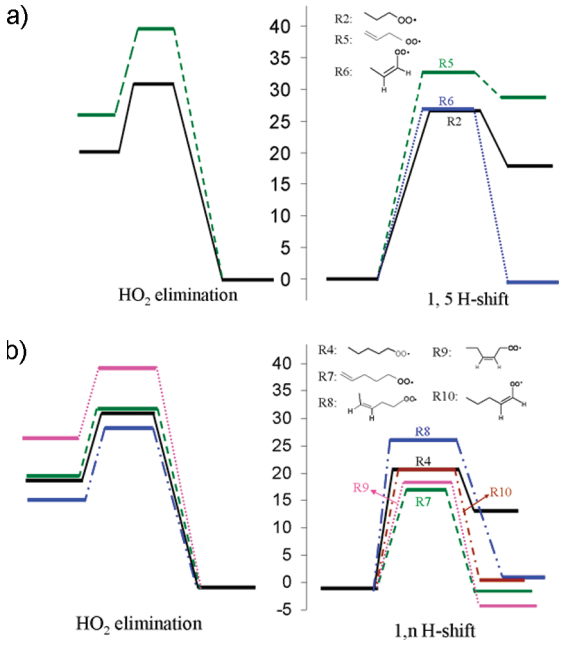

Figure 3. Potential energy diagram for the lowest barrier 1,*n* H-shift (n = 4 for R8, n = 6 for R9, and n = 5 for other reactants) and HO_2 elimination reactions of alkenylperoxy radicals with (a) three carbon atoms and (b) five carbon atoms.

reactions, six singly unsaturated 1-peroxy radicals with three ($C_3H_5O_2$) or five ($C_5H_9O_2$) carbon atoms were chosen as model compounds to be compared with corresponding unsaturated peroxy radicals. These six radicals were denoted as R5−R10 in Scheme 1; the corresponding unsaturated peroxy radicals are R2 and R4. Parts a and b of Figure 3 display potential energy profiles for the two unimolecular reactions for these eight peroxy radicals. The relative energy of each reactant is defined as zero, so that barriers and reaction energies for different species can be compared.

The potential energy profile for HO_2 elimination of the *n*-alkenylperoxy radicals are shown in the left sides of Figure 3a,b. R5 and R9 possess much higher barriers for HO_2 elimination than R2 and R4 (by 8−9 kcal/mol) due to the sp^2 hybridization of the site where the hydrogen atom is removed (recall that R6 and R10, having cis configurations, cannot undergo HO_2 elimination). HO_2 elimination from R8 eliminates the hydrogen atom from an allylic site, and R8 is the only one of these peroxy radicals for which the barrier for HO_2 elimination (28.1 kcal/mol) is comparable to that for the H-shift reaction (barrier of 26.0 kcal/mol). The barrier to HO_2 elimination in R8 is 2.5 kcal/mol lower than that for R4, giving some confirmation to the assumption made by Mehl et al. that the presence of weak allylic C−H bonds lowers the barrier to the direct elimination of HO_2 by 3 kcal/mol. Note that the model of Mehl is designed to treat pressures from 2 to 11 bar and temperatures from 650 to 1100 K. Our master equation calculations indicate that some rate constants are still well into the falloff regime over this pressure and temperature range.

Looking at HO_2 elimination reactions for all species, one can see that the activation barriers closely track the reaction enthalpies. The relationship between the reaction energy, ΔE_{reacn}, and the activation barrier, E_0, can be expressed as

$$E_0 = 9.99 + 1.11\Delta E_{reacn} \quad (5)$$

dx.doi.org/10.1021/jp1111839 |*J. Phys. Chem. A* 2011, 115, 655–663

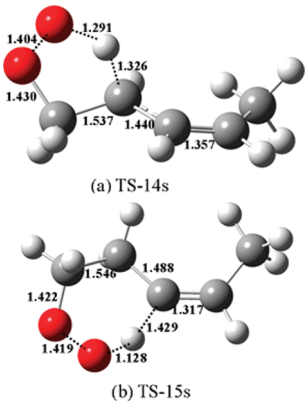

Figure 4. Optimized geometries for the transition state of (a) 1,4 and (b) 1,5 H-shift reactions of 3-pentenyl-1-peroxy radical (R8) at the CBS-QB3 level (internuclear distances in ansgtroms).

(where ΔE_{reacn} and E_0 are in kilocalories per mole). This equation has r^2 = 0.96 and yields a maximum error of 1.65 kcal/mol. The slope of 1.11 in this Evans−Polanyi relationship suggests that the structures of the transition states for HO_2 elimination are late (much closer to the structures of the products than reactants).

Turning now to the 1,5 H-shift of the three-carbon species, one sees from Table 1 and Figure 3a that the H-atom is abstracted from an sp^3-hybridized site in R2 and R6, but from an sp^2-hybridized carbon of R5. As a result, the barrier height for 1,5 H-shift of R5 is about 5 kcal/mol higher than that of R2 and R6. The 1,5 H-shift is not the lowest barrier intramolecular H-shift reaction for R9; the 1,6 H-shift of R9 has a barrier height of 19.8 kcal/mol, versus 26.3 kcal/mol for the 1,5 H-shift. Notice that the 1,5 H-shift only happens from the trans isomer of R9, while the 1,6 H-shift can only occur in the cis isomer, so these two reactions are not actually in competition. As shown in Table 1, the 1,5 H-shift of R8 has the same barrier height (26.0 kcal/mol) as the 1,4 H-shift, but a reaction energy 20.4 kcal/mol higher (only the 1,4 H-shift of R8 is illustrated in Figure 3b). Figure 4 displays the geometries (at B3LYP/6-311G(d,p)) of the saddle points for the 1,4 and 1,5 H-shift reactions of R8, along with the values of the key internuclear distances. The saddle point for the 1,4 H-shift is much earlier than that for the 1,5 H-shift; this earlier transition state is consistent with the 1,4 H-shift being the more exothermic reaction. The sp^2-hybridized site of H-atom abstraction in the 1,5 H-shift of R8 tends to increase the barrier height significantly, making the barrier as high as that for the (strained) five-member ring of the 1,4 H-shift in R8. This is quite consistent with Mehl's prediction that vinylic hydrogens are difficult to abstract.[38]

Among the *n*-pentenyl-1-peroxy radicals shown in Figure 3b, the lowest barrier height belongs to the 1,5 H-shift of R7 with a six-member ring saddle point and an allylic (sp^3-hybridized) site of H-atom abstraction. The barrier heights for 1,5 H-shift of R4 and R10 are indistinguishable. Mehl assumed that the barrier to 1,*n* H-shift transferring an allylic hydrogen is ∼4 kcal/mol less than that for transfer of a secondary alkyl hydrogen; which is consistent with the barrier to the 1,5 H-shift in R7 being 3.4 kcal/mol less than that for R4. Carrying out the same comparison of R10 versus R4 and R6 versus R2 results in differences of −0.1 kcal/mol and +0.2 kcal/mol, respectively; but these comparisons confound two variables, namely, the allylic nature of the site of abstraction with the presence of a C=C double bond in the cyclic transition-state structure. Mehl had suggested that a double bond inside the ring hinders formation of the transition state to the 1,5 H-shift.[38] From the near absence of a difference in the activation barriers for the 1,5 H-shift of R2 and R6, it appears that the extent to which the allylic effect lowers the barrier nearly exactly offsets the rise due to strain energy created by the double bond.

Table 3. Bond Lengths (*B*, Å) and Angles (*A*, degrees) of Saddle Points (T_i) and Resonance-Stabilized Products (P_i) for 1,*n* H-Shift[a] of Reactants R6−R10 at B3LYP/6-311G(d,p)[b]

species	B1	B2	*A*	species	B1	B2	*A*
P6	1.375	1.381	125.2	T6	1.354	1.455	122.4
P7	1.382	1.386	125.3	T7	1.344	1.457	125.1
P8	1.384	1.384	125.5	T8	1.357	1.440	127.4
P9	1.382	1.391	126.3	T9	1.340	1.482	126.5
P10	1.377	1.381	125.6	T10	1.345	1.467	122.8
ally radical	1.383	1.383	125.1				

[a] *n* = 4 for R8, *n* = 6 for R9, and *n* = 5 for other reactants; [b] The site from which the H-atom is abstracted is part of bond B2.

Comparing the potential energy profiles for the 1,5 H-shift of R7 versus R4 in Figure 3, one can see that a 1,*n* H-shift transferring a hydrogen atom from an allylic center lowers the activation barrier by ∼3 kcal/mol but lowers the reaction energy by ∼14 kcal/mol. More generally, the existence of an olefin group next to the site of H-atom abstraction in R6 and the four *n*-pentenyl-1-peroxy radicals yields resonance-stabilized products for intramolecular H-shift reaction, which greatly lowers the reaction energy. The reaction energies for these five systems are 12−16 kcal/mol more negative than those for the corresponding alkylperoxy radicals, yet the activation barriers are not significantly lowered, except for R7. An obvious question is why the strong effect of the allylic group does not appear more in the activation barrier. Comparison of the structures of the saddle points and the resonance-stabilized products at the site of resonance suggests the answer (Table 3). The two C−C bonds in the allylic products show nearly equal bond lengths, as expected, but the saddle point geometries maintain the distinction between single and double bonds. Clearly, the allylic stabilization so noticeable in the products is largely absent in the transition states. This result has been noted previously.[47] While the thermal rate constant for the forward reactions are not much affected, the reduction in reaction energies will tend to reduce the rate constant of the reverse reactions, thereby increasing the importance of processes producing allylic radicals.

A good linear Evans−Polanyi relation is only found for the 1,5 H-shift of R2, R3, R4, R5, R8, and R9, which is described by the following equation with r^2 = 0.96.

$$E_0 = 13.02 + 0.61\Delta E_{reacn} \quad (6)$$

(where ΔE_{reacn} and E_0 are in kilocalories per mole). The slope is close to 0.5, implying that those transition states for 1,5 H-shift are neither early nor late.

B. Kinetics. Figure 5a illustrates the HPL rate constants of 1,5 H-shift and HO_2 elimination as a function of temperature for the three-carbon species R2, R5, and R6 (these and all rate constants presented hereafter include Eckart tunneling). The rate constants of the 1,5 H-shift for R2 and R6 are essentially indistinguishable, while the 1,5 H-shift of R5 has much smaller rate constants due to its much higher barrier height. For

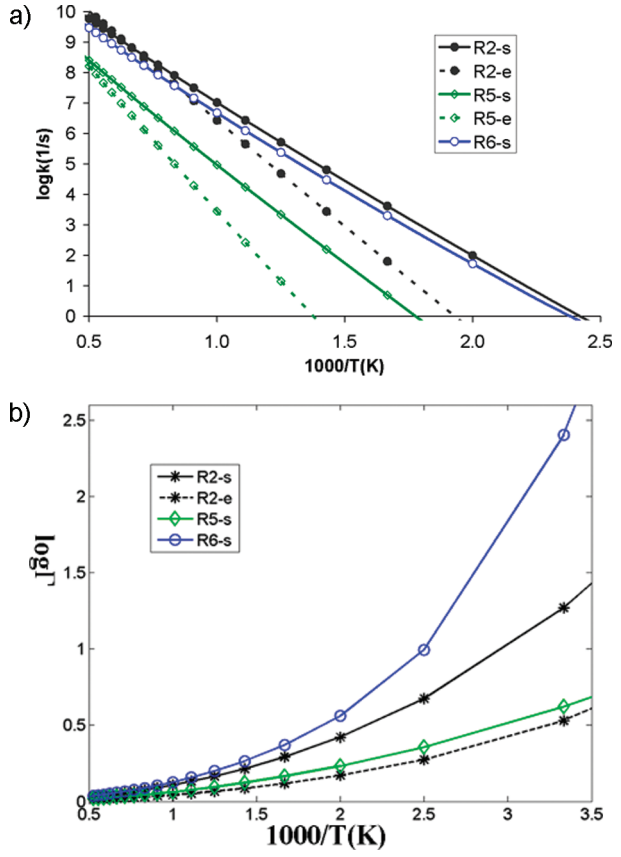

Figure 5. Temperature dependence of (a) HPL rate constants and (b) tunneling correction coefficients of the 1,5 H-shift (labeled s) and HO_2 elimination (labeled e) reactions for 1-propylperoxy and *n*-propenylperoxy radicals.

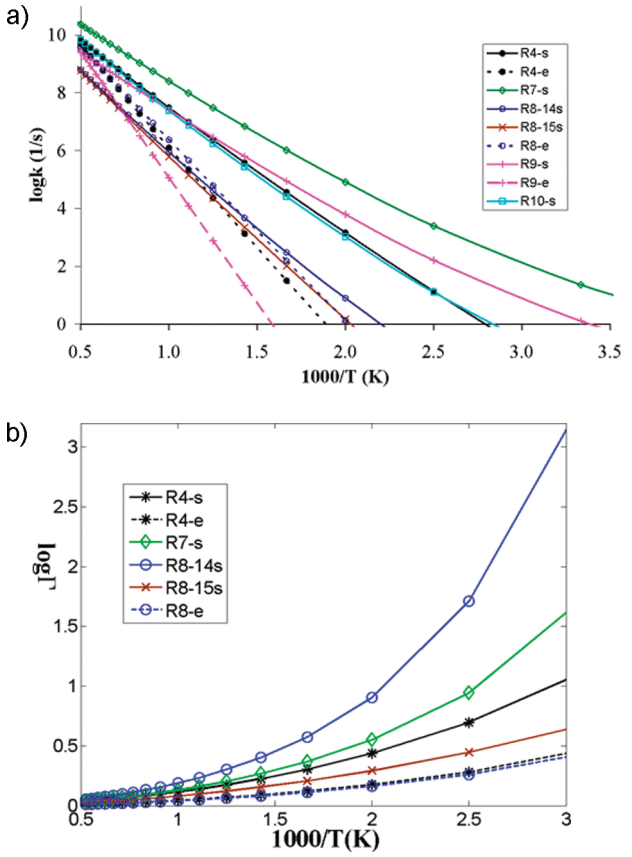

Figure 6. Temperature dependence of (a) HPL rate constants and (b) tunneling correction coefficients of the 1,*n* H-shift ($n = 4$ for R8, $n = 6$ for R9, and $n = 5$ for other species) reactions (labeled s) and selected HO_2 elimination reactions (labeled e) for 1-pentylperoxy and *n*-pentenyl-1-peroxy radicals. The tunneling coefficients for H-shifts of R9 and R10 are indistinguishable from that of R7 and are not explicitly shown.

n-propylperoxy radical (R2), HO_2 elimination never competes with 1,5 H-shift until the temperature exceeds 1500 K. The HPL rate constant with Eckart tunneling (k_{QM}, the quantum mechanical rate constant) and without tunneling (k_{CM}, the classical rate constant) are related to the tunneling correction coefficient (Γ) by the following equation.

$$k_{QM}(T) = \Gamma(T)\, k_{CM}(T) \qquad (7)$$

Figure 5b illustrates the temperature dependence of $\Gamma(T)$ by plotting its logarithm as a function of $1/T$. Clearly, the tunneling effect for HO_2 elimination is much less important than for 1,5 H-shift. This is due largely to the lower imaginary frequencies for HO_2 elimination than those for the 1,5 H-shift, which, in turn, are caused by the higher reduced masses of the imaginary frequencies for HO_2 elimination. As shown in Table 1, although the barrier height for the 1,5 H-shift of R6 is indistinguishable from that of R2, the imaginary frequency is somewhat higher in the case of R6, and the energy of the products is much lower for R6 than R2. As a result, the tunneling effect for the 1,5 H-shift of R6 is much larger than for that of R2, as seen in Figure 5b.

Figure 6 displays the temperature dependence of HPL rate constants and tunneling factors of *n*-pentenyl-1-peroxy radicals. The 1,5 H-shift of R7 has the highest rate constant among all reactions shown in Figure 6a. In the temperature range of 500−1000 K, the rate constant of the 1,5 H-shift of R7 is higher than that of R4 (*n*-pentylperoxy) by 1 order of magnitude. The rate constants for the 1,5 H-shift of R10 and R4 are very similar to each other, but the rate constant for R10 becomes higher than that of R4 at $T < 400$ K. This implies that the tunneling effect is more significant for the 1,5 H-shift of R10 than that of R4. For all species in Figure 6a, HO_2 elimination is not competitive with intramolecular H-shift, except in the case of R8. The rate constant for HO_2 elimination of R8 is slightly higher than that for the more favored (1,4) H-shift of R8 for $T > 700$ K. The rate constant of the 1,4 H-shift of R8 falls off relatively slowly with decreasing temperature because of tunneling. The rate constant of HO_2 elimination for R7 is indistinguishable from that for R4, and, therefore, is not shown in Figure 6a.

Figure 6b illustrates the temperature dependence of tunneling coefficients for H-shift and HO_2 elimination of *n*-pentylperoxy and *n*-pentenyl-1-peroxy radicals. The tunneling coefficient curves for H-shifts of R9 and R10 are indistinguishable from that of R7, and so are not shown in Figure 6b. Some tunneling coefficients for HO_2 elimination are also absent from the figure to avoid duplication. The intramolecular H-shifts of the four *n*-pentenyl-1-peroxy radicals have more significant tunneling effects than that of *n*-pentylperoxy radical (R4), except the 1,5 H-shift of R8. The saddle point of the 1,4 H-shift for R8 has a particularly high imaginary frequency; consequently, the Eckart tunneling correction for this reaction of R8 is particularly large. The fact that 1,*n* H-shifts of some *n*-pentenyl-1-peroxy radicals

dx.doi.org/10.1021/jp1111839 |*J. Phys. Chem. A* 2011, 115, 655–663

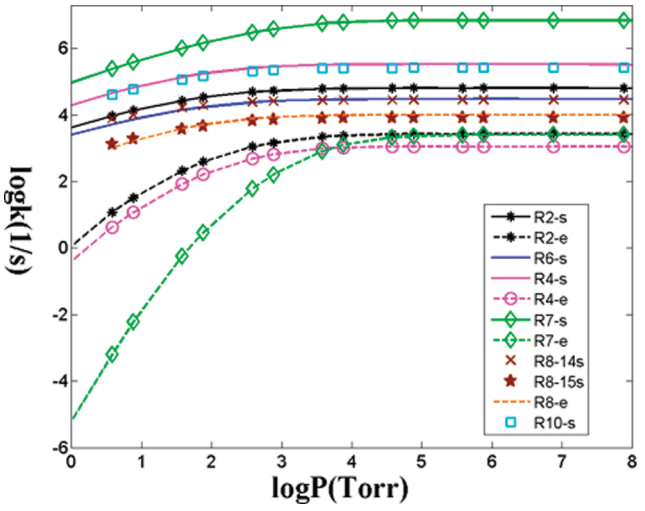

Figure 7. Pressure dependence of rate constants for the 1,*n* H-shift (n = 4 for R8 and n = 5 for other species) and HO_2 elimination reactions for selected *n*-alkenyl-1-peroxy radicals (R6, R7, R8, and R10) and the corresponding alkylperoxy radicals (R2 and R4).

are roughly thermoneutral rather than endothermic creates a large tunneling effect, thereby increasing the rate constant above the classical value at medium to low temperatures.

Autoignition chemistry occurs or is studied at a wide range of pressures but is most important at a narrow range of temperatures near 700 K. The rate constants as a function of a wide range of P and T are presented in the Supporting Information. Since this work focuses on the autoignition process, the following discussion of the pressure dependence of HO_2 elimination and isomerization only considers 700 K. The decomposition of R5 and R9 leads to allylic radicals and O_2, which are lower in energy than the barriers to the intramolecular H-shift and HO_2 elimination reactions. As a result, these reactions are unlikely to compete with decomposition, and the falloff curves for those two unimolecular reactions will not be computed in this work. It should be noted that these calculations of $k(P,T)$ assume a Boltzmann distribution of energy whose high-energy tail is depleted by reaction at pressures below the HPL, which is not the generally the case for chemically activated peroxy radicals formed from the R· + O_2 reaction.

Figure 7 shows the pressure dependence of the two competing unimolecular reactions for *n*-propenyl-1-peroxy and *n*-pentenyl-1-peroxy radicals and the corresponding alkylperoxy radicals. Both reactions are considered in competition with one another, so that the reaction with the lower barrier tends to decrease the rate constant for the reaction with the higher barrier and extend the pressure range over which the higher barrier reaction is in the falloff region. Since the HO_2 elimination reactions tend to have the higher barriers, the rate constants for most HO_2 elimination reactions shown in Figure 7 depend more on pressure than intramolecular H-shift. The exception is R8, for which the HO_2 elimination and H-shift reactions possess very similar barriers and display very similar pressure dependences. The thermal rate constants for all three reactions of R8 reach 90% of the HPL values at 1 atm. The pressure dependence of the rate constants for HO_2 elimination is particularly dramatic for R7 and R9. For example, at 1 atm, the rate constant of HO_2 elimination for R7 is only 6% of its HPL rate constant. This difference occurs because the much faster H-shift reaction reduces the population of highly activated molecules (the high-energy tail of the Boltzmann distribution) that can undergo HO_2 elimination. The result is that the fast intramolecular H-shift reaction depresses the rate constant of HO_2 elimination in the falloff region.

4. CONCLUSIONS

Using quantum chemistry together with statistical rate theory, the effect of the presence and position of olefin functional groups on the kinetics of key unimolecular reactions of peroxy radicals has been investigated. The lowest energy conformers for 10 selected peroxy radicals were determined by CBS-QB3 calculations. Calculations on alkylperoxy radicals were used to evaluate sources of uncertainty in the computational method. This work represents the first ab initio and kinetic study of two key classes of unimolecular reactions for *n*-pentenylperoxy radicals. We conclude that, for alkenylperoxy radicals, the 1,*n* H-shift reaction with a resonance-stabilized (allylic) product, induced by an olefin group located β to the site of abstraction, tends to be the lowest barrier intramolecular H-shift channel. The allylic products of the 1,*n* H-shift for alkenylperoxy radicals lead to very low energy QOOH structures and, consequently, a larger tunneling effect. sp^2 hybrization of the site of H-atom abstraction greatly increases barriers for both internal H-shift and direct HO_2 elimination. Tunneling corrections appear to be much larger for 1,*n* H-shift than for HO_2 elimination, but this conclusion relies on the use of the Eckart formula, which is not necessarily reliable. The pressure dependence of HO_2 elimination is strongly affected by the presence of a much faster 1,*n* H-shift channel.

■ ASSOCIATED CONTENT

Ⓢ Supporting Information. Tables listing Cartesian coordinates (Å) of all stationary points for the reactions, Lennard-Jones parameters, vibrational modes treated as hindered rotors, HPL rate constants and tunneling correction coefficients, and pressure-dependent rate constants at 500, 700, 1000, 1500, and 2000 K. This material is available free of charge via the Internet at http://pubs.acs.org.

■ AUTHOR INFORMATION

Corresponding Author

*Tel.: 315-470-6596. Fax: 315-470-6856. E-mail: tsdibble@syr.edu.

■ ACKNOWLEDGMENT

We thank Dr. Miyoshi for his kind help in installing and using the UNIMOL and GPOP program suites, and two anonymous reviewers for their extensive contributions toward improving this work. This work was supported by the U.S. Department of Energy under Grant DE-SC0002511.

■ REFERENCES

(1) Agarwal, K. *Prog. Energy Combust. Sci.* **2007**, *33*, 233.

(2) Risher, J. F.; Rhodes, S. W. *Toxicological profile for fuel oils*, U. S. Department of Heath and Human Services, Agency for Toxic Substances and Disease Registry, June 1995.

(3) Van Gerpen, J. *The Basics of Diesel Engines and Diesel Fuels. In the Biodiesel Handbook*; Knothe, G, Van Gerpen, J., Krahl, J., Eds.; AOCS Press: Champaign, IL, 2005 (http://www.uidaho.edu/bioenergy/BiodieselEd/publication/03.pdf).

(4) Benson, S. W. *Prog. Energy Combust. Sci.* **1981**, *7*, 125.
(5) Compton, R. G.; Hancock, G.; Pilling, M. J. *Comprehensive Chemical Kinetics: Low-Temperature Combustion and Autoignition*; Elsevier Science: Amsterdam, 1997.
(6) Hayes, C. J.; Merle, J. K.; Hadad, C. M. *Adv. Phys. Org. Chem.* **2008**, *43*, 79.
(7) Buda, F.; Bounaceur, R.; Warth, V.; Glaude, P. A.; Fournet, R.; Battin-Leclerc, F. *Combust. Flame* **2005**, *142*, 170.
(8) Suzaki, K.; Kanno, N.; Tonokura, K.; Koshi, M.; Tsuchiya, K.; Tezaki, A. *Chem. Phys. Lett.* **2006**, *425*, 179.
(9) Baldwin, R. R.; Pickering, I. A.; Walker, R. W. *J. Chem. Soc., Faraday Trans. 1* **1980**, *76*, 2374.
(10) Wagner, A. F.; Slagle, I. R.; Sarzynski, D.; Gutman, D. *J. Phys Chem.* **1990**, *94*, 1853.
(11) Pilling, M. J.; Robertson, S. H.; Seakins, P. W. *J. Chem. Soc., Faraday Trans.* **1995**, *91*, 4179.
(12) Hunter, T. B.; Litzinger, T. A.; Wang, H.; Frenklach, M. *Combust. Flame* **1996**, *104*, 505.
(13) Clifford, E. P.; Farrell, J. T.; DeSain, J. D.; Taatjes, C. A. *J. Phys. Chem. A* **2000**, *104*, 11549.
(14) Rienstra-Kiracofe, J. C.; Allen, W. D.; Schaefer, H. F., III. *J. Phys. Chem. A* **2000**, *104*, 9823.
(15) Kaiser, E. W. *J. Phys. Chem. A* **2002**, *106*, 1256.
(16) Naik, C. V.; Dean, A. M. *Combust. Flame* **2006**, *145*, 16.
(17) Wilke, J. J.; Allen, W. D.; Schaefer, H. F., III. *J. Chem. Phys.* **2008**, *128*, 074308.
(18) Miller, J. A.; Klippenstein, S. J.; Robertson, S. H. *Proc. Combust. Inst.* **2000**, *28*, 1479.
(19) Miller, J. A.; Klippenstein, S. J. *Int. J. Chem. Kinet.* **2001**, *33*, 654.
(20) Sheng, C. Y.; Bozzelli, J. W.; Dean, A. M.; Chang, A. Y. *J. Phys. Chem. A* **2002**, *106*, 7276.
(21) Blanksby, S. J.; Ramond, T. M.; Davico, G. E.; Nimlos, M. R.; Kato, S.; Bierbaum, V. M.; Lineberger, W. C.; Ellison, G. B.; Okumura, M. *J. Am. Chem. Soc.* **2001**, *123*, 9585.
(22) DeSain, J. D.; Clifford, E. P.; Taatjes, C. A. *J. Phys. Chem. A* **2001**, *105*, 3205.
(23) DeSain, J. D.; Taatjes, C. A.; Miller, J. A.; Klippenstein, S. J.; Hahn, D. K. *Faraday Discuss.* **2001**, *119*, 101.
(24) DeSain, J. D.; Klippenstein, S. J.; Miller, J. A.; Taatjes, C. A. *J. Phys. Chem. A* **2003**, *107*, 4415.
(25) Estupiñán, E. G.; Klippenstein, S. J.; Taatjes, C. A. *J. Phys. Chem. B* **2005**, *109*, 8374.
(26) Huang, H.; Merthe, D. J.; Zádor, J.; Jusinski, L. E.; Taatjes, C. A. *Proc. Combust. Inst.* **2011**, *33*, 293−299.
(27) Taatjes, C. A. *J. Phys. Chem. A* **2006**, *110*, 4299.
(28) Merle, J. K.; Hayes, C. J.; Zalyubovsky, S. J.; Glover, B. G.; Miller, T. A.; Hadad, C. M. *J. Phys. Chem. A* **2005**, *109*, 3637.
(29) Zhu, L.; Bozzelli, J. W.; Kardos, L. M. *J. Phys. Chem. A* **2007**, *111*, 6361.
(30) Westbrook, C. K.; Pitz, W. J.; Boercjerm, J. E.; Curran, H. J.; Griffiths, J. F.; Mohamed, C.; Ribaucour, M. *Proc. Combust. Inst.* **2002**, *29*, 1311.
(31) Glaude, P. A.; Conraud, V.; Fournet, R.; Battin-Leclerc, F.; Côme, G. M.; Scachi, G.; Dagaut, P.; Cathonnet, M. *Energy Fuels* **2002**, *16*, 1186.
(32) Sharma, S.; Raman, S.; Green, W. H. *J. Phys. Chem. A* **2010**, *1114*, 5689.
(33) Davis, A. C.; Francisco, J. S. *J. Phys. Chem. A* **2010**, *114*, 11492.
(34) Lee, J.; Bozzelli, J. W. *Proc. Combust. Inst.* **2005**, *30*, 1015.
(35) Miyoshi, A. *Int. J. Chem. Kinet.* **2010**, *42*, 273.
(36) Bounaceur, R.; Warth, V.; Sirjean, B.; Glaude, P. A.; Fournet, R.; Battin-Leclerc, F. *Proc. Combust. Inst.* **2009**, *32*, 387.
(37) Firestone, D. *Physical and Chemical Characteristics of Oils, Fats, and Waxes*, 2nd ed.; AOCS Press: Washingotn, DC, 2006.
(38) Mehl, M.; Vanhove, G.; Pitz, W. J.; Ranzi, E. *Combust. Flame* **2008**, *155*, 756.
(39) Viskolcz, B.; Lendvay, G.; Seres, L. *J. Phys. Chem. A* **1997**, *101*, 7119.
(40) Chan, W.-T.; Hamilton, I. P.; Pritchard, H. O. *J. Chem. Soc., Faraday Trans.* **1998**, *94*, 2303.
(41) *Spartan'08*; Wavefunction: Irvine, CA, 2006−2009.
(42) Zhao, Y.; Truhlar, D. G. *J. Phys. Chem. A* **2008**, *112*, 1095.
(43) Zhao, Y.; Truhlar, D. G. *J. Phys. Chem. A* **2005**, *109*, 5656.
(44) Zhao, Y.; Truhlar, D. G. *Acc. Chem. Res.* **2008**, *41*, 157.
(45) Montgomery, J. A., Jr.; Frisch, M. J.; Ochterski, J. W.; Petersson, G. A. *J. Chem. Phys.* **1999**, *110*, 2822.
(46) Carstensen, H.-H.; Naik, C. V.; Dean, A. M. *J. Phys. Chem. A* **2005**, *109*, 2264.
(47) Peeters, J.; Nguyen, T. L.; Vereecken, L. *Phys. Chem. Chem. Phys.* **2009**, *11*, 5935.
(48) Da Silva, G.; Graham, C.; Wang, Z. F. *Environ. Sci. Technol.* **2010**, *44*, 250.
(49) Scott, A. P.; Radom, L. *J. Phys. Chem.* **1996**, *100*, 16502.
(50) Frisch, M. J.; Trucks, G. W.; Schlegel, H. B.; Scuseria, G. E.; Robb, M. A.; Cheeseman, J. R.; Scalmani, G.; Barone, V.; Mennucci, B.; Petersson, G. A.; Nakatsuji, H.; Caricato, M.; Li, X.; Hratchian, H. P.; Izmaylov, A. F.; Bloino, J.; Zheng, G.; Sonnenberg, J. L.; Hada, M.; Ehara, M.; Toyota, K.; Fukuda, R.; Hasegawa, J.; Ishida, M.; Nakajima, T.; Honda, Y.; Kitao, O.; Nakai, H.; Vreven, T.; Montgomery, J. A., Jr.; Peralta, J. E.; Ogliaro, F.; Bearpark, M.; Heyd, J. J.; Brothers, E.; Kudin, K. N.; Staroverov, V. N.; Kobayashi, R.; Normand, J.; Raghavachari, K.; Rendell, A.; Burant, J. C.; Iyengar, S. S.; Tomasi, J.; Cossi, M.; Rega, N.; Millam, J. M.; Klene, M.; Knox, J. E.; Cross, J. B.; Bakken, V.; Adamo, C.; Jaramillo, J.; Gomperts, R.; Stratmann, R. E.; Yazyev, O.; Austin, A. J.; Cammi, R.; Pomelli, C.; Ochterski, J. W.; Martin, R. L.; Morokuma, K.; Zakrzewski, V. G.; Voth, G. A.; Salvador, P.; Dannenberg, J. J.; Dapprich, S.; Daniels, A. D.; Farkas, Ö.; Foresman, J. B.; Ortiz, J. V.; Cioslowski, J.; , Fox, D. J. *Gaussian 09*, Revision A.1; Gaussian: Wallingford, CT, 2009.
(51) Lewis, F. D.; Weitz, E. *Acc. Chem. Res.* **1985**, *18*, 188.
(52) Gilbert, R. G.; Smith, S. C.; Jordan, M. J. T. *UNIMOL Program Suit*; School of Chemistry, Sydney University: Sydney, Australia, 1993.
(53) Miyoshi, A. UNIMOL package, http://www.frad.t.u-tokyo.ac.jp/∼miyoshi/ssumes/index.html.
(54) Miyoshi, A. GPOP package is available at http://www.frad.t.u-tokyo.ac.jp/∼miyoshi/gpop/.
(55) Gilbert, R. G.; Smith, S. C. *Theory of Unimolecular and Recombination Reactions*; Blackwell: Oxford, U.K., 1990.
(56) Reid, R. C.; Sherwood, T. K. *The Properties of Gases and Liquids: Their Estimation and Correlation*; McGraw-Hill: New York, 1958.
(57) *CRC Handbook of Chemistry and Physics*, 90th ed.; 2009−2010 (http://www.hbcpnetbase.com/).
(58) Eckart, C. *Phys. Rev.* **1930**, *35*, 1303.
(59) Garett, B. C.; Truhlar, D. G. *J. Phys. Chem.* **1979**, *83*, 2921.
(60) Pitzer, K. S.; Gwinn, W. D. *J. Chem. Phys.* **1942**, *10*, 428.
(61) Vereecken, L.; Nguyen, T. L.; Hermans, I.; Peeters, J. *Chem. Phys. Lett.* **2004**, *393*, 432.
(62) Razavy, M. *Quantum Theory of Tunneling World*; Scientific: Singapore, 2003.
(63) Merrick, J. P.; Morgan, D.; Radom, L. *J. Phys. Chem. A* **2007**, *111*, 11683.
(64) Miller, J. A.; Kliipenstein, S. J. *J. Phys. Chem. A* **2006**, *110*, 10528.
(65) Kliipenstein, S. J.; Miller, J. A. *J. Phys. Chem. A* **2002**, *106*, 9267.
(66) Hirschfelder, J. O.; Wigner, E. *J. Chem. Phys.* **1939**, *7*, 616.
(67) Isaacson, A. D.; Truhlar, D. G; Rai, S. N.; Steckler, R.; Hancock, G. C.; Garrett, B. C.; Redmon, M. J. *Comput. Phys. Commun.* **1987**, *47*, 91.
(68) Peles, D. N; Thoburn, J. D. *J. Org. Chem.* **2008**, *73*, 3135.